High-speed mapping of synaptic connectivity using photostimulation in Channelrhodopsin-2 transgenic mice

H. Wang*, J. Peca*†, M. Matsuzaki‡§, K. Matsuzaki‡, J. Noguchi‡, L. Qiu*, D. Wang*, F. Zhang¶, E. Boyden¶, K. Deisseroth¶, H. Kasai‡, W. C. Hall*, G. Feng*‖, and G. J. Augustine*‡‖

*Department of Neurobiology, Duke University, Durham, NC 27710; †Center for Neuroscience and Cell Biology, University of Coimbra, 3004-517 Coimbra; Portugal; ‡Division of Biophysics, Center for Disease Biology and Integrative Medicine, Faculty of Medicine, University of Tokyo, Tokyo 113-0033, Japan; §Precursory Research for Embryonic Science and Technology, Japan Science and Technology Agency, Saitama 332-0012, Japan; and ¶Department of Bioengineering, Stanford University, Palo Alto, CA 94305

Edited by Richard W. Tsien, Stanford University School of Medicine, Stanford, CA, and approved March 16, 2007 (received for review January 15, 2007)

To permit rapid optical control of brain activity, we have engineered multiple lines of transgenic mice that express the light-activated cation channel Channelrhodopsin-2 (ChR2) in subsets of neurons. Illumination of ChR2-positive neurons in brain slices produced photocurrents that generated action potentials within milliseconds and with precisely timed latencies. The number of light-evoked action potentials could be controlled by varying either the amplitude or duration of illumination. Furthermore, the frequency of light-evoked action potentials could be precisely controlled up to 30 Hz. Photostimulation also could evoke synaptic transmission between neurons, and, by scanning with a small laser light spot, we were able to map the spatial distribution of synaptic circuits connecting neurons within living cerebral cortex. We conclude that ChR2 is a genetically based photostimulation technology that permits analysis of neural circuits with high spatial and temporal resolution in transgenic mammals.

brain networks | cortical circuitry | synaptic transmission

Although the electrode has long been the preferred tool for controlling neuronal electrical activity, this method of stimulation has a number of shortcomings, including mechanical damage inflicted on the target tissue, limited spatial resolution with extracellular electrodes, and a limited population of activated neurons (typically one cell) when using intracellular electrodes. An alternative way to stimulate neurons is to use light as a source of energy. Three approaches have been used for photostimulation: light-mediated uncaging of neurotransmitters to activate endogenous (1, 2) or heterologous receptors (3, 4), modification of ion channels to induce light sensitivity (5), and introduction of naturally occurring light-sensitive channels and receptors (6, 7).

A recent addition to the repertoire of light-sensitive channels is Channelrhodopsin-2 (ChR2), a seven-transmembrane ion channel from the algae *Chlamydomonas reinhardtii* that exhibits a nonselective cation flux when exposed to blue-green light (8–10). ChR2 was first engineered for delivery to cultured hippocampal neurons (11), followed by a mammalian cell line (12), *Caenorhabditis elegans* (13), *Drosophila* (14), and, more recently, the retina of living mice (15). ChR2-based photostimulation offers many advantages, such as high spatial resolution, millisecond precision, lack of toxicity, and amenability to genetic targeting (11).

In previous work, we mapped synaptic circuitry (2) and neurotransmitter receptors (16) with optical methods and genetically engineered mouse lines that express fluorescent proteins in specific cell types within living mammalian nervous systems (17). Here, we combine these approaches with ChR2 photostimulation (11) and report successful generation of transgenic mice expressing ChR2 fused to yellow fluorescent protein (YFP). This approach allows the expression of both activator (ChR2) and reporter (YFP) in well defined subsets of cells for the physiological manipulation of neuronal activity. In acute slices, light-induced currents could be elicited readily and caused depolarization sufficient to generate action potentials and evoked synaptic responses with millisecond temporal resolution. No cofactor (such as retinal) needed to be added, a crucial feature for *in vivo* experimentation. Together, these data demonstrate that ChR2 offers a convenient means of mapping functional neuronal circuitry in the mammalian brain.

Results

Neuronal Expression of Channelrhodopsin-2-YFP in Transgenic Mice. Regulatory elements from the mouse thy1.2 gene (Fig. 1*A*) were used to drive neuron-specific expression of ChR2-YFP. Differences in the position and/or copy numbers of transgene insertion produced patterns of expression in subsets of neurons that varied among the different mouse lines but were consistent within a particular line (17). From our initial 10 transgenic founders, seven lines were established that expressed ChR2. Four (lines 9, 15, 18, 19) had high levels of expression in multiple regions of the brain, as visualized by YFP fluorescence. ChR2-positive cells include layer V cortical neurons (Fig. 1 *B–D*), CA and CA3 pyramidal neurons in the hippocampus (Fig. 1 *E* and *F*), mossy fibers in the cerebellum (Fig. 1 *C* and *G*), and neurons in various regions of the thalamus, midbrain, and lower brainstem (Fig. 1 *B* and *C*). Additional images of ChR2 expression patterns are shown in supporting information (SI) Fig. 7. ChR2 was targeted to the plasma membrane and the intensity of the YFP fluorescence signal was highest where the membrane had a high surface/volume ratio, such as in dendrites and axons (e.g., Fig. 1*D*).

ChR2 mice were viable, bred normally, and had no obvious anatomical defects or behavioral abnormalities. To determine whether ChR2 expression alters the functional properties of the neuron in the absence of illumination, we used patch clamp recordings to compare the membrane properties of ChR2-positive cortical layer V pyramidal neurons in slices from line-18 mice, which had the strongest CNS expression of ChR2, with the properties of ChR2-negative neurons in the same slices. No significant differences were found between the electrical properties of ChR2-

Author contributions: H.W., J.P., and M.M. contributed equally to this work; H.K., W.C.H., G.F., and G.J.A. designed research; H.W., J.P., and M.M. performed research; K.M., J.N., L.Q., D.W., F.Z., E.B., K.D., and G.F. contributed new reagents/analytic tools; H.W., J.P., and M.M. analyzed data; and H.W., K.D., W.C.H., G.F., and G.J.A. wrote the paper.

The authors declare no conflict of interest.

This article is a PNAS Direct Submission.

Abbreviations: ChR2, Channelrhodopsin-2; CNQX, 6-cyano-7-nitroquinoxaline-2,3-dione; IPSC, inhibitory postsynaptic current; YFP, yellow fluorescent protein.

‖To whom correspondence may be addressed. E-mail: georgea@neuro.duke.edu or feng@neuro.duke.edu.

This article contains supporting information online at www.pnas.org/cgi/content/full/0700384104/DC1.

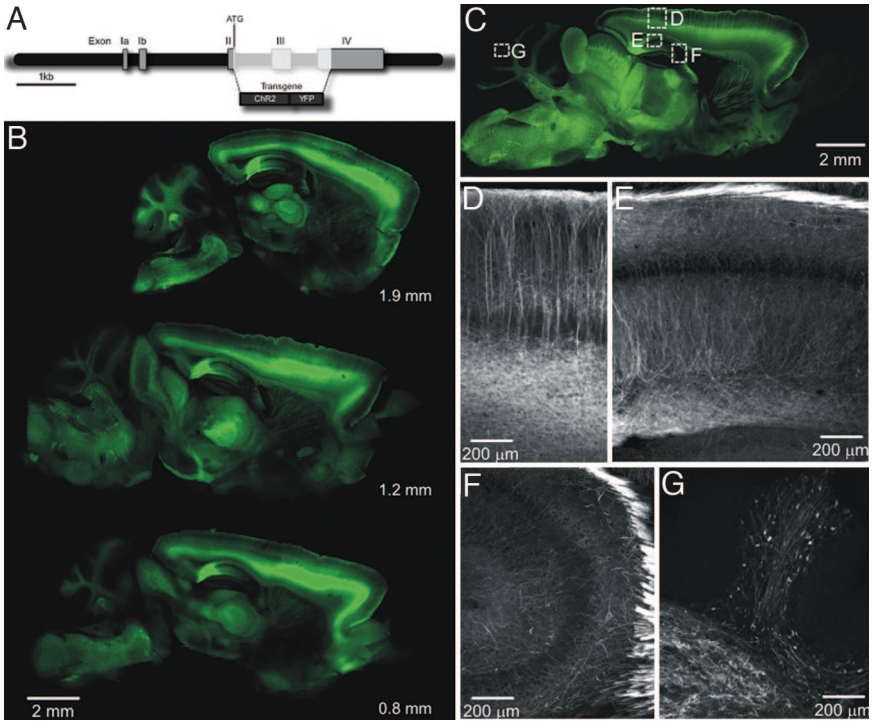

Fig. 1. Transgenic expression of Chr2-YFP in mouse brain. (*A*) Thy1-Chr2-YFP construct. cDNA encoding a Chr2-YFP fusion protein was placed under the control of the regulatory elements of the mouse Thy1.2 gene. (*B*) Serial parasagittal sections from an adult transgenic mouse brain (line 9). Distance from the midline is indicated below each YFP fluorescence image. (*C*) Expression of Chr2-YFP in various regions of an adult line 18 mouse brain. Rectangles indicate areas enlarged in *D*–*G* below. (*D*) In the cortex, layer V neurons express high levels of Chr2-YFP and their apical dendrites are clearly labeled. (*E* and *F*) In the hippocampus both CA1 and CA3 neurons express ChR2-YFP. (*G*) Cerebellar mossy fibers show high levels of Chr2-YFP expression.

positive and ChR2-negative cells (Table 1), indicating that ChR2 affects neither resting properties nor action potentials.

Photostimulation of ChR2-Expressing Neurons. Illumination of ChR2-positive pyramidal neurons produced photocurrents with very short latencies. These currents were examined in cortical slices treated with blockers of glutamate [10 μM 6-cyano-7-nitroquinoxaline-2,3-dione (CNQX) and 50 μM 2-amino-5-phosphonovaleric acid] and GABA (50 μM picrotoxin or 10 μM GABAzine) receptors, to prevent the generation of light-evoked postsynaptic responses (see below). We first used light spots illuminating large areas of the slices ($\approx$0.4 mm^2). Under such conditions, 1-s long light pulses (465–495 nm, 9.2 mW/mm^2) caused ChR2-positive neurons to generate inward currents at a holding potential of -70 mV (Fig. 2*A*, middle trace). In 10 experiments, the mean peak current induced by such photostimuli was 557 $\pm$ 153 pA. In contrast, no currents were generated during illumination of neurons in slices from wild-type mice (Fig. 2*A*, bottom trace; $n = 10$), indicating that the light responses were due to expression of ChR2.

Increasing light luminance increased photocurrent amplitude (Fig. 2*B*). The relationship between photostimulus intensity and peak amplitude of the current response could be described by the Hill equation (solid line in Fig. 2*C*):

$$Y = I_{max}\frac{X^n}{K^n + X^n} \quad [1]$$

where X is light intensity and K represents the half-maximal light sensitivity of the ChR2 (0.84 $\pm$ 0.2 mW/mm^2). I_{max}, the maximum current, was 642 $\pm$ 38 pA and n, the Hill coefficient, was 0.76 $\pm$ 0.1. This relationship presumably arises from progressive recruitment of ChR2 activation, with saturation reflecting activation of all available ChR2 channels. The Hill coefficient of nearly 1 indicates that absorption of a single photon is sufficient for activation of ChR2. These observations are consistent with previous studies of ChR2 expressed in neurons (11, 12, 15).

During prolonged illumination, ChR2-dependent photocurrents reached their peak rapidly and then inactivated. The mean time to the peak of the current was 12.0 $\pm$ 0.1 ms ($n = 10$) and the mean time constant for current inactivation was 48 $\pm$ 0.9 ms ($n = 10$) at a light luminance of 9.2 mW/mm^2. For durations ranging from 2–8 ms, increasing light duration caused large increases in the peak amplitude of photocurrents (Fig. 2*D*). In contrast, further prolonging flash duration did not increase the peak amplitude of the photocurrent (Fig. 2*E*) but did increase the total charge associated with photostimulation. The relationship between light duration and peak amplitude of the photocurrent was very sharp (Fig. 2*F*) and also could be described by the Hill equation. The light duration required for half-maximal photoactivation (K) was 3.2 ms, indicating rapid activation of ChR2 by light under our conditions. The Hill coefficient, n, was 7.7, reflecting the steep time course of ChR2 channel activation.

ChR2 could very rapidly depolarize ChR2-positive neurons to fire action potentials. Whereas very dim light flashes caused

Table 1. Comparison of electrical properties of ChR2 expressing neurons

Genotype	Resting potential, mV	Input resistance, MΩ	Threshold, mV	Action potential duration, ms	Action potential amplitude, mV	Action potential overshoot, mV
ChR2$^-$	-58.3 ± 1.8	126 ± 13	-29.6 ± 2.2	1.02 ± 0.11	93.4 ± 5.9	35.7 ± 1.2
ChR2$^+$	-61.4 ± 1.4	110 ± 4.5	-35.4 ± 2.2	1.11 ± 0.09	99.5 ± 7.1	38.1 ± 0.2

Sample size is 10 cells for each group. There was no statistically significant difference ($P > 0.05$) in the mean value of any parameter between the two types of neurons.

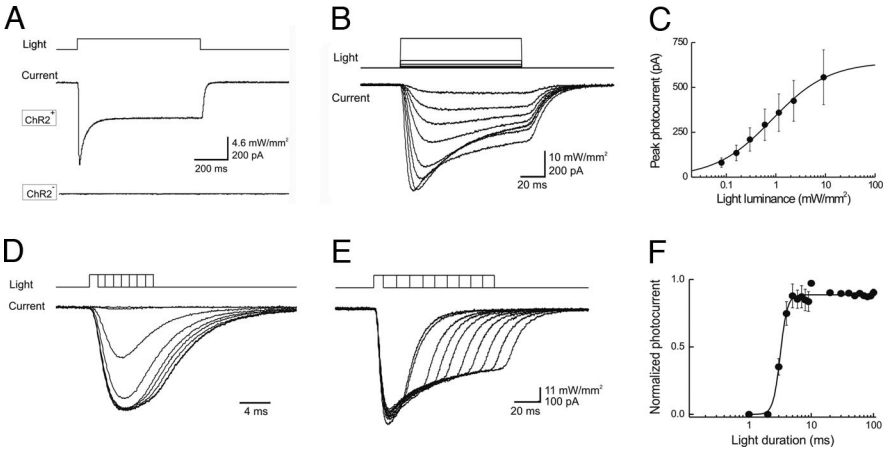

Fig. 2. Illumination evokes photocurrents in ChR2-positive cortical neurons. (*A*) Prolonged light flash (top trace) generated a photocurrent (middle trace) in a neuron that expressed ChR2. No photocurrent was observed in a ChR2-negative neuron from a wild-type mouse (bottom trace). (*B*) The peak amplitude of photocurrents (lower trace) increased as a function of light intensity (upper trace). (*C*) Relationship between photocurrent amplitude and light intensity (100-ms duration); points indicate means ± SEM for seven neurons. Curve is a fit of the Hill equation. (*D* and *E*) Photocurrent (bottom traces) varied with light duration (top traces). (*D*) Responses to brief light pulses (1- to 8-ms durations). (*E*) Responses to longer duration flashes (10- to 100-ms durations). (*F*) Relationship between photocurrent amplitude and photostimulus duration (9.2 mW/mm^2 luminance). Curve is fit of the Hill equation.

subthreshold depolarizations, brighter flashes caused larger depolarizations that evoked action potentials (Fig. 3*A*). The mean latency from light onset to the peak of the first action potential was 6.1 ± 0.1 ms (n = 10). Action potential jitter, defined as the standard deviation of the spike latency, was 0.3 ms, indicating high temporal precision. The first action potentials in the light-induced trains often were followed by an after-depolarization that generated a smaller secondary spike; these responses were observed in both ChR2-positive and ChR2-negative neurons when current was injected through the patch pipette (data not shown), indicating that the after-depolarization is an intrinsic property of these cells (18).

Action potential number was proportional to light intensity and saturated at high intensities (Fig. 3*B*). Fits of the Hill equation indicated a half-maximal light intensity of 0.49 ± 0.1 mW/mm^2 and a Hill coefficient of 0.82 ± 0.1, again indicating that a single photon is required for activation of ChR2. The maximum number of action potentials was 25.4 ± 1.2 for 1-s duration light flashes. This is very similar to the maximum action potential frequency of 26.6 ± 3.5 Hz (n = 8) evoked by direct injection of large currents, indicating that ChR2 photostimulation can trigger action potentials at a rate that is limited by the intrinsic properties of the pyramidal neurons.

The frequency response of ChR2 photostimulation was examined by varying the rate of light pulses (4-ms duration). In the cell shown in Fig. 3*C*, action potentials were evoked by every photostimulus up to 30 Hz and the probability of success was greatly reduced at higher frequencies. On average, such ChR2-positive cells could follow reliably at frequencies up to 30 Hz and the probability of generating action potentials was reduced to 50% at 35 Hz (Fig. 3*D*).

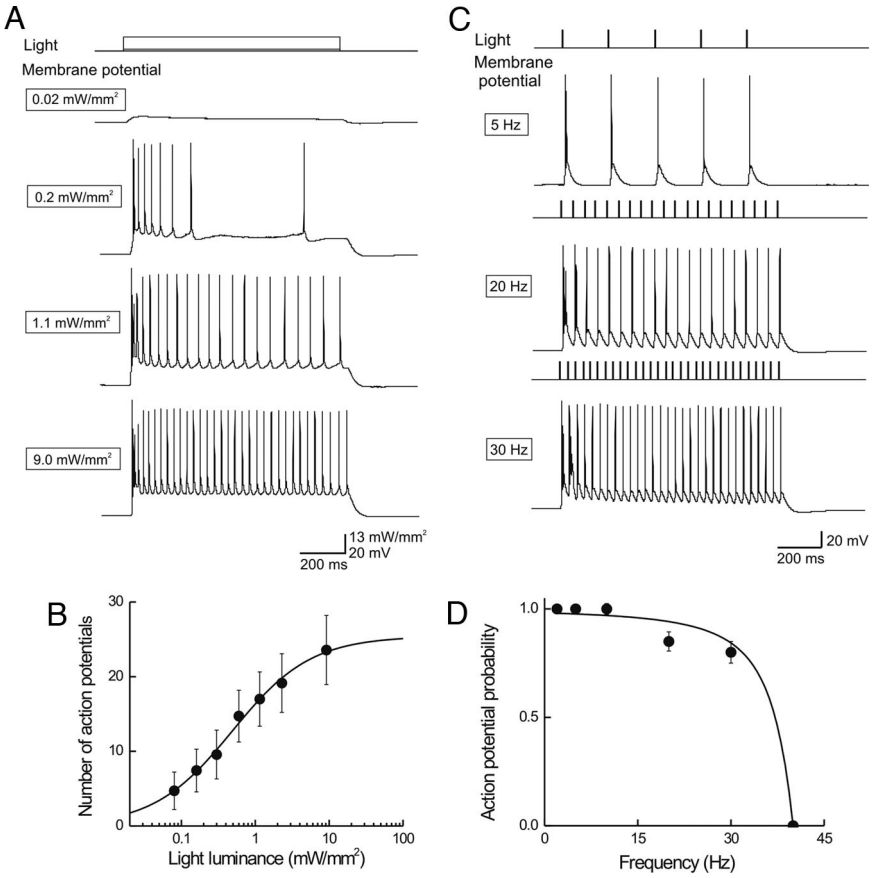

Fig. 3. Illumination controls number and frequency of action potentials. (*A*) Light of varying luminance elicited graded changes in membrane potential and varying numbers of action potentials. (*B*) Relationship between light intensity and number of light-evoked action potentials (n = 4). Curve is fit of the Hill equation. (*C*) Varying the frequency of brief light flashes (4 ms duration; 9.2 mW/mm^2) caused proportional changes in action potential frequency. (*D*) Mean probability of evoked action potentials decreased with light pulse frequency (n = 4). Curve is a Lorentzian function, with a roll-off frequency of 35 Hz.

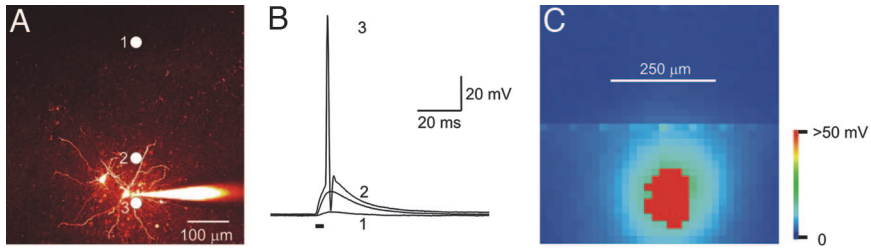

Fig. 4. Mapping light sensitivity of pyramidal neuron. (*A*) Structure of a pyramidal neuron filled with Alexa 594 dye that was dialyzed from a patch pipette (to the right). Here, and in subsequent figures, the top of the image is closest to the pial surface. Circles indicate locations where photoresponses in *B* were evoked. (*B*) Changes in membrane potential evoked by light spots (488 nm; 48 mW/mm^2) positioned at the sites indicated in *A*. Only illumination near the cell body evoked an action potential (trace 3). Bar indicates time of illumination. (*C*) Scanning the light spot across the specimen revealed locations where light-induced depolarizations were evoked; pseudocolor scale at right indicates the amplitude of these responses. Red reflects action potentials.

To define the location of light sensitivity, we used a laser light spot (1–100 μm diameter; 458- or 488-nm wavelength) to illuminate small regions of ChR2-positive cortical pyramidal neurons. Individual neurons were filled with the fluorescent tracer dye, Alexa 594 (50 μM), to visualize cell morphology (Fig. 4*A*) and the light spot (4-ms duration) was scanned in a two-dimensional array over the surface of the cell. Although depolarizing responses could be elicited when the light spot was positioned over virtually any region of the cell, responses were largest when the light spot was located in the immediate vicinity of the neuronal cell body (Fig. 4*B*). Even at the highest light levels (up to 70 mW/mm^2), action potentials could be evoked only when the light spot was located near the cell body (red area in Fig. 4*C*). The area in which action potentials could be evoked was ≈100 μm in diameter, with a mean area of 11,000 ± 3,000 μm^2 (n = 3). The higher sensitivity of the somatic region presumably arises from its relatively large surface area.

Mapping Neural Circuitry by ChR2. We next determined whether ChR2 photostimulation permits activation and functional mapping of neural circuits. The approach was to use small light spots to stimulate presynaptic neurons expressing ChR2, as in Fig. 4, while monitoring postsynaptic responses in neurons that did not express ChR2. For this purpose, we used slices from line 9 mice and patch clamped layer V-VI interneurons, which rarely expressed ChR2. Fig. 5*A* illustrates the widespread distribution of ChR2 expression in layer VI of a living cortical slice and Fig. 5*B* indicates a dye-filled interneuron within this field of view. The interneuron did not express ChR2, evident as the lack of YFP fluorescence and the absence of immediate, direct responses to light (see next paragraph). Bright illumination (24 mW/mm^2) at various locations within the slice elicited synaptic responses in the interneuron (Fig. 5*C*). In the example shown in Fig. 5*C*, illumination at site 1, >250 μm away from the cell body of the interneuron, produced no detectable response. Illumination nearer the interneuron, such as sites 2 and 3, elicited inward synaptic currents. Given the results shown in Fig. 4, these sites presumably indicate the location of the somata/proximal dendrites of ChR2-positive presynaptic neurons. By scanning the light spot in two dimensions, it was possible to map the spatial distribution of all ChR2-positive neurons that provide synaptic input to this layer VI interneuron. The resulting map is shown in Fig. 5*D*, with the amplitude of the evoked synaptic currents encoded into the pseudocolor scale shown on the right. This map reveals pronounced spatial gradients in synaptic input, with the largest responses evoked when the light stimulus was within ≈200 μm of the interneuron. Similar results were obtained in a total of eight experiments. Thus, the ChR2 photostimulation technique detects the presence of local synaptic circuits produced by ChR2-expressing neurons innervating cortical interneurons and precisely defines the spatial range of these circuits.

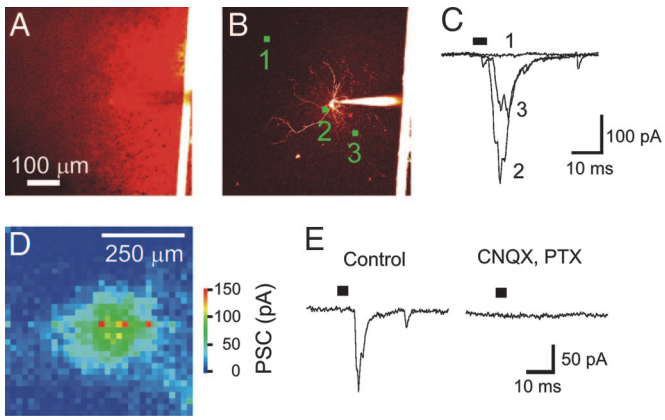

Fig. 5. Mapping of local excitatory circuits innervating cortical interneurons. (*A*) Image of ChR2-YFP fluorescence in layer VI of a living cortical slice. Bright structure on right side of image is thread used to anchor slice. (*B*) Dye-filled interneuron, with circles indicating locations where photoresponses in *C* were evoked. (*C*) Light-induced postsynaptic currents (holding potential = 70 mV), detected when a light spot (488 nm; 24 mW/mm^2) was positioned at the locations indicated in *B*. (*D*) Map of spatial distribution of locations where light evoked synaptic currents; the magnitude of these currents is indicated by the pseudocolor scale at right. (*E*) Light-evoked currents (*Left*) were blocked by coapplication of 10 μM CNQX and 50 μM picrotoxin (PTX) (*Right*), indicating that they resulted from synaptic activity. Bars in *C* and *E* indicate time of illumination.

Several criteria demonstrated that these light-induced currents originated from synaptic activity rather than direct photostimulation. First, they appeared several milliseconds after the light stimulus (bar in Fig. 5*C*), whereas the direct photocurrents occurred with negligible delay (Fig. 2*D*). Second, the responses often had multiple peaks (traces 2 and 3 in Fig. 5*C*), presumably because of activation of multiple presynaptic neurons (or repetitive firing in a single presynaptic cell), whereas the direct photocurrents developed smoothly and never had multiple peaks. Third, the responses were eliminated after slices were exposed to a mixture of drugs that block postsynaptic receptors (10 μM CNQX and 50 μM picrotoxin), as shown in Fig. 5*E*. Finally, these responses were blocked by tetrodotoxin (1 μM; data not shown), indicating that they were evoked by action potentials in presynaptic neurons rather than from ChR2, which is insensitive to this toxin.

Data shown in *SI Text* demonstrates that maps of synaptic circuitry produced by ChR2-based photostimulation were stable over measurement intervals as long as 20–30 min and that these maps were relatively insensitive to the intensity of the light spot (SI Fig. 8). These features indicate that mapping of neural circuitry by ChR2 can be both practical and reproducible.

Although most layer V/VI pyramidal cells appeared to be ChR2-positive in line 9, in a few experiments we were able to obtain recordings of postsynaptic responses from ChR2-negative pyramidal neurons (Fig. 6*A*). In these cases, we could map the synaptic input of these cells without the complication of currents resulting from direct photostimulation of the pyramidal cell (Fig. 6*B*). As was the case for interneurons, responses detected at the usual holding potential of −70 mV (Fig. 6*C*) largely consisted of excitatory postsynaptic currents (see below). In every instance (n = 3), maps of excitatory inputs to pyramidal cells were qualitatively different

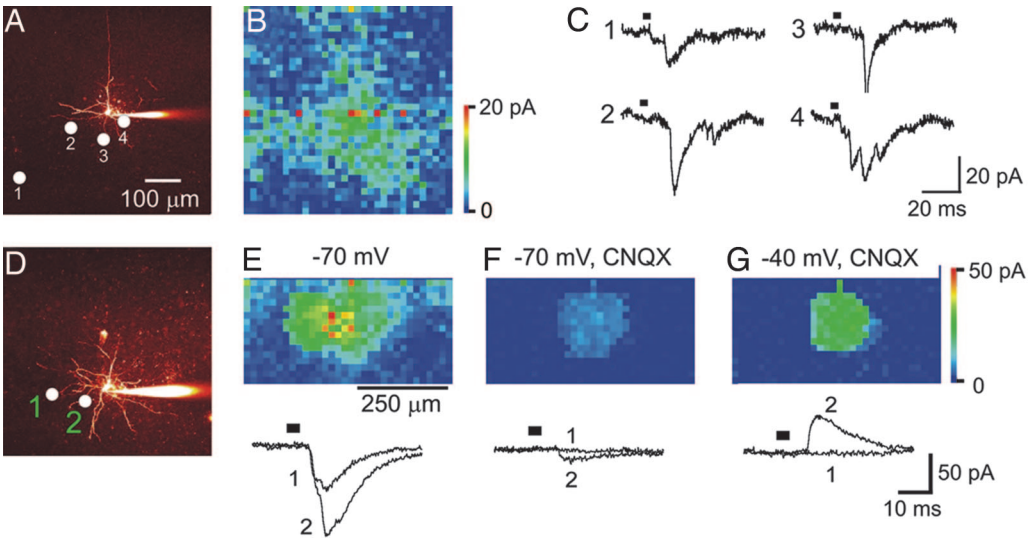

Fig. 6. Properties of cortical microcircuits. (*A*) Fluorescence image of dye-filled layer VI pyramidal neuron. (*B*) Map of synaptic circuit innervating the pyramidal neuron shown in *A*. (*C*) Traces indicate excitatory postsynaptic currents (holding potential = −70 mV) measured when the light spot was positioned at the indicated locations in *A*. (*D*) Fluorescence image of dye-filled layer VI pyramidal neuron; circles indicate locations where light-evoked synaptic responses shown at the bottom of *E* were evoked. (*E*) Map of excitatory synaptic inputs innervating the neuron shown in *D*. Traces below the map indicate excitatory postsynaptic currents, measured at a holding potential of −70 mV, when the light spot was positioned at the locations indicated in *D*. (*F*) Treatment with 10 μM CNQX almost completely blocked the responses measured at −70 mV (compare with *E*), indicating that the responses in *E* are largely glutamatergic excitatory postsynaptic currents. (*G*) Same conditions as in (*E*) except that the postsynaptic membrane potential was changed to −40 mV, to reveal outward IPSCs (traces below). Comparison of *E* with *G* shows that inhibitory and excitatory inputs have different spatial distributions on the same cell. Bars in *C* and *E*–*G* indicate time of illumination.

from those measured for interneurons within the same layers of the cortex. For example, the map for the layer VI pyramidal cell shown in Fig. 6*B* is substantially broader than for the interneurons shown in Fig. 5*D* and SI Fig. 8 *B* and *E*. The mean area of the region of synaptic input to interneurons was 58,000 ± 15,000 μm^2 ($n = 8$), whereas the inputs for pyramidal cells were larger but could not be quantified because they typically extended beyond the 500-μm width of a photostimulation field. Even though the local circuits innervating interneurons usually were circular or elliptical, those of pyramidal cells were irregular in shape. Although there are diverse types of pyramidal neurons and interneurons, our measurements indicate that the local excitatory drive of interneurons generally is more spatially restricted than that of pyramidal cells.

Even though the thy-1 promoter largely expressed ChR2 in pyramidal neurons, in some cases the presence of light-induced inhibitory postsynaptic currents (IPSCs) indicated that cortical interneurons were also being photostimulated. Fig. 6*D* shows a layer VI pyramidal neuron that had excitatory synaptic input distributed in the pattern described above (Fig. 6*E*). At a holding potential of −70 mV, near the equilibrium potential for chloride ions, inward postsynaptic currents could be evoked at many locations, such as sites 1 and 2 (Fig. 6*E Lower*). Treatment with the glutamate receptor antagonist, CNQX (10 μM), greatly reduced these currents, confirming that they were predominantly excitatory postsynaptic currents (Fig. 6*F*). In the continued presence of CNQX, shifting the holding potential to −40 mV (away from the chloride equilibrium potential) then revealed outward currents representing IPSCs that had been concealed at −70 mV (Fig. 6*G Lower*). With this manipulation, we could determine that ChR2-driven inhibitory inputs onto this pyramidal neuron were more restricted in their spatial extent than the ChR2-driven excitatory inputs (compare Fig. 6*G* with Fig. 6*E*). We likewise found that inhibitory circuits innervating interneurons were smaller than the excitatory circuits (data not shown). In both cases, this difference likely arises from the sparser expression of ChR2 in interneurons compared with pyramidal cells in line 9. In fact, the uniform amplitude of the IPSCs shown in Fig. 6*G* indicates that they may arise from photostimulation of a single inhibitory neuron. Given that these uniform IPSCs were generated by scanning the light spot over >70 pixels, this result further demonstrates the consistency and reproducibility of ChR2 photostimulation of synaptic activity.

Discussion

Illumination of ChR2-positive neurons in cortical slices produced rapid photocurrents that could elicit action potentials. The timing, number, and spatial location of these action potentials could be controlled precisely by light, allowing functional mapping of cortical circuits. Thus, ChR2 is an efficient and reliable means of using light to activate and map neural circuits, even after chronic expression.

Several groups recently have developed optical methods to control neuronal activity (3–6, 11, 19). These methods provide complementary advantages and disadvantages, allowing selection of a photostimulation method based on the needs of the genetic model organism or the experimental arrangement. Application of ChR2 methodology to the mammalian brain combines the optimal features of several approaches, allowing genetic targeting and cofactor independence and millisecond-scale precision that can match the time scale of circuit activity.

Our experiments are the first to use the power of ChR2 to map neural connectivity in the mammalian brain. This complements recent demonstrations of the use of ChR2 to restore visual responses in mice with impaired vision (15) and to evoke behavioral responses in worms and flies (12, 14). Through the use of ChR2 photostimulation, we visualized the spatial distribution of synaptic circuits in the cerebral cortex. Glutamate uncaging has also been used for this purpose (1, 2, 20, 21); ChR2-based circuit mapping avoids the large direct responses invariably produced when uncaging glutamate near a postsynaptic neuron, which can obscure the contributions of very local inputs (21). In addition, genetic targeting of ChR2 allows exclusive stimulation of defined cellular subsets and avoids the need for addition of the caged glutamate, facilitating photostimulation *in vivo* (22).

As an initial test of the efficacy of ChR2-based photostimulation for circuit mapping, we expressed ChR2 behind the Thy-1 promoter. In this case, ChR2 expression was so strong that responses were limited by the intrinsic properties of the pyramidal neuron

rather than by the properties of ChR2; this might not be the case for promoters that yield weaker expression of ChR2. ChR2 photostimulation was so effective that action potentials were elicited by light spots positioned over either the cell body or primary dendrites of pyramidal cells (Fig. 4). Thus, the effective spatial resolution for mapping connectivity was on the order of 100 μm. The distribution of ChR2 expression also is critical for circuit mapping. For the line of mice that we used for circuit mapping (line 9), cortical expression of ChR2 was widespread and largely restricted to pyramidal neurons. We found that this population of cells produced more widespread excitation of pyramidal neurons than of interneurons. Future targeting of ChR2 to more restricted populations of neurons should allow further refinement of such input maps. The use of imaging methods to monitor the responses of populations of postsynaptic neurons (23) should further enhance the efficacy of ChR2-based circuit mapping.

Determining the contribution of discrete populations of neurons to information processing within the circuitry of the intact brain has long been a central goal of neuroscience. However, defining the contribution of the activity of particular neuronal populations to intact neural circuits has been an elusive goal, in part because it has been difficult to selectively stimulate populations of neurons. Our work indicates that ChR2 photostimulation is a powerful addition to the genetic tools currently available for manipulating and mapping neuronal circuits in brain tissue.

Materials and Methods

Generation of ChR2 Transgenic Mice. ChR2-EYFP (11) was cloned into the mouse thy1.2 vector (17, 24). Digested DNA fragments containing the Thy1-ChR2-YFP sequence were gel-purified and transgenic mice were generated by using standard pronuclear injection (25). Of 19 pups born, 10 were identified as positive through tail DNA PCR, using primers for thy1.2 and ChR2 (Thy1F1, TCTGAGTGGCAAAGGACCTTAGG: ChR2R1, GAAGATGACCTTGACGTATCCG), which amplify a 600-bp fragment. The transgenic lines generated were backcrossed to C57BL/6.

Anatomy. To assess the expression of ChR2-YFP, three adults from each line were anesthetized with an overdose of halothane and perfused transcardially with 0.1 M phosphate saline buffer followed by 4% paraformaldehyde. Brains were cut into 50-μm-thick slices on a vibratome. Fluorescence images ($\times$4) were obtained with an AxioImager microscope (Zeiss, Thornwood, NY) or a Nikon (Melville, NY) confocal microscope.

Brain-Slice Recording and Photostimulation. Cortical parasagittal slices, 250–350 μm thick, were prepared from 13- to 36-d-old transgenic mice (2, 16). Animal procedures were approved by the Animal Use Committees of Duke University and the University of Tokyo. Electrical responses were recorded with an Axoclamp 2B amplifier (Axon Instruments, Foster City, CA), acquired with Clampfit (Axon Instruments), and analyzed with Igor Pro.

Recording pipettes had resistances of 2–7 MΩ and contained 130 mM K-gluconate, 2 mM NaCl, 4 mM $MgCl_2$, 20 mM Hepes, 4 mM Na_2ATP, 0.4 mM NaGTP, and 250 μM K-EGTA (pH 7.3). The extracellular solution consisted of 125 mM NaCl, 2.5 mM KCl, 2 mM $CaCl_2$, 1 or 1.3 mM $MgCl_2$, 20 mM dextrose or D-glucose, 1.25 mM NaH_2PO_4, and 26 mM $NaHCO_3$, (pH 7.4 after bubbling with 95% O_2/5% CO_2). GABAzine (SR-95531; 10 μM; Sigma, St. Louis, MO) or 50 μM picrotoxin (Wako, Osaka, Japan), CNQX (10 μM; Sigma) and 2-amino-5-phosphonovaleric acid (50 μM; Sigma) sometimes were added to block synaptic transmission. Retinal or retinol (1 μM) sometimes were included in the extracellular solution, but had no detectable effect on responses to light. A junction potential of 10 mV was taken into account when reporting membrane potentials. Experiments were performed at room temperature (21–24°C).

Slices were examined on an upright epifluorescence microscope (Eclipse E600-FN; Nikon). To identify ChR2 expressing neurons, the YFP fused to ChR2 was excited (465–495 nm light) and emitted fluorescence (515–555 nm) was detected with a CoolSNAP-fx camera (Photometrics, Tucson, AZ). ChR2 was excited with bandpass filtered light pulses (465–495 nm) from the same arc lamp and pulse duration was controlled by an electronic shutter (Uniblitz T132; Vincent, Rochester, NY).

In optical mapping experiments, a laser scanning microscope (FV1000; Olympus, Tokyo, Japan) equipped with a water-immersion objective lens (XLUMPlanFI20XW, numerical aperture of 0.95) was used to image and photostimulate. A light spot was produced by the 488-nm or 458-nm emission lines of an Argon ion laser and scanned in a two-dimensional array (16). The region scanned consisted of a 32 $\times$ 32 array of pixels (18-μm diameter). Scanning was done in a pseudorandom sequence, to ensure that the distance between two successive pixels was $>$270 μm, with a 100-ms time interval between successive photostimulation events. The intracellular solution used in these experiments consisted of 120 mM potassium gluconate, 20 mM KCl, 10 mM disodium phosphocreatine, 50 μM Alexa 594, 4 mM Mg-ATP, 0.3 mM NaGTP, and 10 mM Hepes-KOH (pH 7.3). For imaging of Alexa-594 filled neurons, the microscope used a mode-locked femtosecond-pulse Ti:sapphire laser (MaiTaiHP; Spectra Physics, Mountain View, CA) tuned to 830 nm. The free-radical scavenger Trolox (200 μM; Aldrich, Milwaukee, WI) was added to the extracellular solution to minimize phototoxicity.

We thank K. Berglund, Y. Li, and K. Tanaka for help and for their comments on a draft of this paper. This work was supported by National Institutes of Health Grants (to K.D., W.C.H., G.F., and G.J.A.), Grants-in-Aid from the Ministry of Education, Culture, Sports, Science, and Technology of Japan (to H.K. and M.M.) and Nano Bio Integration, the University of Tokyo (H.K., M.M., and J.N.).

1. Callaway EM, Katz LC (1993) *Proc Natl Acad Sci USA* 90:7661–7665.
2. Pettit DL, Helms, MC, Lee, P, Augustine GJ, and Hall WC (1999) *J Neurophysiol* 81:1424–1427.
3. Zemelman BV, Nesnas N, Lee GA, Miesenbock G (2003) *Proc Natl Acad Sci USA* 100:1352–1357.
4. Lima SQ, Miesenbock G (2005) *Cell* 121:141–152.
5. Banghart M, Borges K, Isacoff E, Trauner D, Kramer RH (2004) *Nat Neurosci* 7:1381–1386.
6. Zemelman BV, Lee GA, Ng M, Miesenbock G (2002) *Neuron* 33:15–22.
7. Li, X. et al. (2005) *Proc Natl Acad Sci USA* 102:17816–17821.
8. Suzuki T, Yamasaki K, Fujita S, Oda K, Iseki M, Yoshida K, Watanabe M, Daiyasu H, Toh H, Asamizu E, *et al.* (2003) *Biochem Biophys Res Comm* 301:711–717.
9. Sineshchekov OA, Jung KH, Spudich JL (2002) *Proc Natl Acad Sci USA* 99:8689–8694.
10. Nagel G, Szellas T, Huhn W, Kateriya S, Adeishvili N, Berthold P, Ollig D, Hegemann P, Bamberg E (2003) *Proc Natl Acad Sci USA* 100:13940–13945.
11. Boyden ES, Zhang F, Bamberg E, Nagel G, Deisseroth K (2005) *Nat Neurosci* 8:1263–1268.
12. Ishizuka T, Kakuda M, Araki R, Yawo H (2006) *Neurosci Res* 54:85–94.
13. Nagel G, Brauner M, Liewald JF, Adeishvili N, Bamberg E, Gottschalk A (2005) *Curr Biol* 15:2279–2284.
14. Schroll C, Riemensperger T, Bucher D, Ehmer J, Voller T, Erbguth K, Gerber B, Hendel T, Nagel G, Buchner E, Fiala A (2006) *Curr Biol* 16:1741–1747.
15. Bi A, Cui J, Ma YP, Olshevskaya E, Pu M, Dizhoor AM, Pan ZH (2006) *Neuron* 50:23–33.
16. Matsuzaki M, Honkura N, Ellis-Davies GC, Kasai H (2004) *Nature* 429:761–766.
17. Feng G, Mellor RH, Bernstein M, Keller-Peck C, Nguyen QT, Wallace M, Nerbonne JM, Lichtman JW, Sanes JR (2000) *Neuron* 28:41–51.
18. McCormick DA, Connors BW, Lighthall JW, Prince DA (1985) *J Neurophysiol* 54:782–806.
19. Volgraf M, Gorostiza P, Numano R, Kramer RH, Isacoff EY, Trauner D (2006) *Nat Chem Biol* 2:47–52.
20. Dantzker JL, Callaway EM (2000) *Nat Neurosci* 3:701–707.
21. Schubert D, Kotter R, Zilles K, Luhmann HJ, Staiger JF (2003) *J Neurosci* 23:2961–2970.
22. Arenkiel BR, Peca J, Davison IG, Feliciano C, Deisseroth K, Augustine GJ, Ehlers MD, Feng G (2007) *Neuron*, in press.
23. Ohki K, Chung S, Kara P, Hubener M, Bonhoeffer T, Reid RC (2006) *Nature* 442:925–928.
24. Caroni P (1997) *J Neurosci Methods* 71:3–9.
25. Feng G, Lu J, Gross J (2004) *Methods Mol Med* 99:255–267.